Coupling of TiO_2 and ZnO with metal sulfides (CuS AND ZnS) for applications in solar cells

J. C. Solis Cortazar, A. K. López Matus, L. Rojas Blanco, G. Pérez Hernández, I. Zamudio Torres, B. L. Pérez Escobar, R. Castillo Palomera, E. Ramírez Morales*
Academic Division of Engineering and Architecture, Juarez Autonomous University of Tabasco, Road Cunduacán-Jalpa KM. 1. Col. La Esmeralda CP. 86690. Cunduacán, Tabasco, México

TiO_2 and ZnO films were synthesized by the dip-coating method. The coupling of thin films of metal sulfides: CuS and ZnS by thermal evaporation in each semiconductor oxide was analyzed. TiO_2, CuS/TiO_2, ZnS/TiO_2, ZnO, CuS/ZnO, and ZnS/ZnO samples were analyzed by X-ray diffraction, Raman microscopy, atomic force microscopy, UV-Vis spectroscopy, and photoresponse. The optical and morphological analysis revealed that the CuS/TiO_2 and CuS/ZnO samples present better properties than the pristine samples. This was attributed to the fact that their absorption edges move to lower energy regions and their roughness increases refraction, so there is a greater photoelectric response due to the accumulation of photo-injected electrons in the conduction band.

(Received October 10, 2023; Accepted April 2, 2024)

Keywords: TiO_2, ZnO, Heterojunctions, Sol-gel, Thin films, Metal sulfides

1. Introduction

The manufacture of photovoltaic devices using semiconductor materials has had a great impact because it is a highly efficient and environmentally friendly technology [1]. Among the various semiconductor materials that are applied to photovoltaic devices are mainly TiO_2 [2] and ZnO [3], which are chemically stable, cheap, non-toxic and easy to manufacture [4], [5], [6]. However, the disadvantage of these semiconductors is their high charge carrier recombination [7]. Therefore, layers of metal sulfides have been incorporated to improve the optical properties [8]. Among the most used metal sulfides as an electron transport layer are: CuS and ZnS whose energy gaps are 2.24 and 3.68 eV, respectively [9], [10]. In addition, it has been reported that the incorporation of this sulfide layer provides a significant improvement in corrosion resistance [11]. In the present study the synthesis and deposition of TiO_2 and ZnO films using the dip coating method is reported. After the deposit of the oxides, metallic sulfides of CuS and ZnS were coupled by the evaporation method. With the coupling, the aim is to improve the optical properties of the heterojunctions and thus have an impact on the reduction of the recombination processes of the photogenerated electron/hole pairs (e^-/h^+), which affect the efficiency of solar cells. The optical and electrical characterization of thin films allows the analysis of transmittance, refraction, and response to visible light.

2. Experimental

2.1. Materials and methods

For the sol gel synthesis of TiO_2, 6.5 ml of titanium tetrabutoxide were stirred for 1 hour at room temperature: ($Ti[OC(CH_3)_3]_4$, Sigma-Aldrich, 97%), 1.35 ml of H_2O, 1 ml of hydrochloric acid (HCl, J.T. Baker, 36.7%) and 55 ml of ethanol (CH_3CH_2OH, Meyer 99.5%) [12]. On the

* Corresponding author: eriking10@hotmail.com
https://doi.org/10.15251/DJNB.2024.192.493

other hand, for ZnO, zinc acetate dihydrate ($Zn(CH_3COO)_2 \cdot 2H_2O$, J.T. Baker 99%), ethyl alcohol (CH_3CH_2OH, Meyer 99.5%) and diethanolamine ($HN(CH_2CH_2OH)$ Sigma-Aldrich, 99%) were stirred for 1 hour at 60°C and was kept at rest for 48 hours [13]. A molar ratio between $HN(CH_2CH_2OH)_2$ and $Zn(CH_3COO)_2 \cdot 2H_2O$ of 1:0.75 was used. The TiO_2 and ZnO films were manufactured by the dip-coating method, with 3-minute immersion at 1 mm/s; repeating the procedure to obtain bilayers and drying each film for 2 min at 200 °C in an oxidizing atmosphere. To obtain the CuS/ZnO, CuS/TiO_2, ZnS/ZnO and ZnS/TiO_2 heterojunctions, the sulfides were deposited by thermal evaporation on the oxide films using CuS and ZnS (Sigma-Aldrich 99.9%) at a pressure of 10-6 torr.

2.2. Characterization

The materials were characterized using a Rigaku X-ray diffractometer (λ (Cuk_α)=1.54056 Å). Raman spectra were obtained with a HORIBA XploRA PLUS spectrometer with a 532 nm laser as Nd-YAG excitation source. An Agilent-8453 UV-Vis spectrophotometer was used to determine optical transmittance. An XE7 Park system atomic force microscope was used to obtain the topography. For the analysis of the photoresponse of the films, an AUTOLAB PGSTAT80N galvanostat potentiostat was used with an applied voltage of 1 V for 200 seconds with 50 W halogen lamp lighting intermittently every 10 seconds.

3. Results and discussions

3.1. X-ray diffraction

Figure 1-a) shows TiO_2, CuS/TiO_2, and ZnS/TiO_2 diffractograms. The characteristic TiO_2 peaks are observed, and the main planes corresponding to the anatase phase (JCPDS 21-1272) [14], [15] are indicated. Figure 1-d) shows the diffractograms of ZnO, CuS/ZnO, and ZnS/ZnO. The characteristic planes of the hexagonal wurtzite (JCPDS 36-1451) phase of ZnO are observed in (100), (002), (101), (102), (110), (103), (112), and (201) located at 31.84°, 34.36°, 36.32°, 47.44°, 56.72°, 62.84°, 68.04° and 69.16°, respectively [16].

The diffractograms were compared with JCPDS 06-0464 for CuS and JCPDS 75-1534 for ZnS. It is observed that the incorporation of CuS and ZnS in the TiO_2 and ZnO films causes the shifting of some planes to the left and right, as shown in Figures 1-b), c), e), and f). It is attributed to the likenesses between the positions of their diffraction planes and the electronic electronegativity of the TiO_2, ZnO, CuS, and ZnS compounds. In addition, because Ti^{4+} (0.61 Å), Zn^{2+} (0.75 Å), and Cu^{2+} (0.69 Å) have different ionic radii, strong TiO_2 and ZnO signals are promoted in the diffractograms [17], [18]. The amorphous region in the diffractograms is attributed to the glass substrate [19].

Crystal sizes (D) were calculated using the Scherrer equation [20]:

$$D = \frac{K\lambda}{\beta \cos\theta} \quad (1)$$

K is a shape factor (0.9), λ is the wavelength, β is the width at half height of the principal plane (101), and θ is the Bragg angle. The values obtained for the TiO_2 and ZnO crystals are summarized in Table 1.

Table 1. Structural Patterns of TiO_2 and ZnO Crystal.

Sample	Crystallite size (nm)	Lattice red (Å)	
		$\boldsymbol{a}$	$\boldsymbol{c}$
TiO_2	13	3.78550	9.69787
CuS/TiO_2	15	3.78700	9.62896
ZnS/TiO_2	13	3.79326	9.55701
ZnO	19	3.74459	3.82262
CuS/ZnO	15	3.74909	3.82098
ZnS/ZnO	17	3.74814	3.82114

The results show changes in the crystallite size and the lattice parameters, attributed to the stacking of the crystals [21]. Moreover, the distortion that can occur as a result of the substitution of Ti^{4+} ions by Zn^{2+} in the structure, which, due to having similar ionic radii, do not change the TiO_2 phase [21], [22].

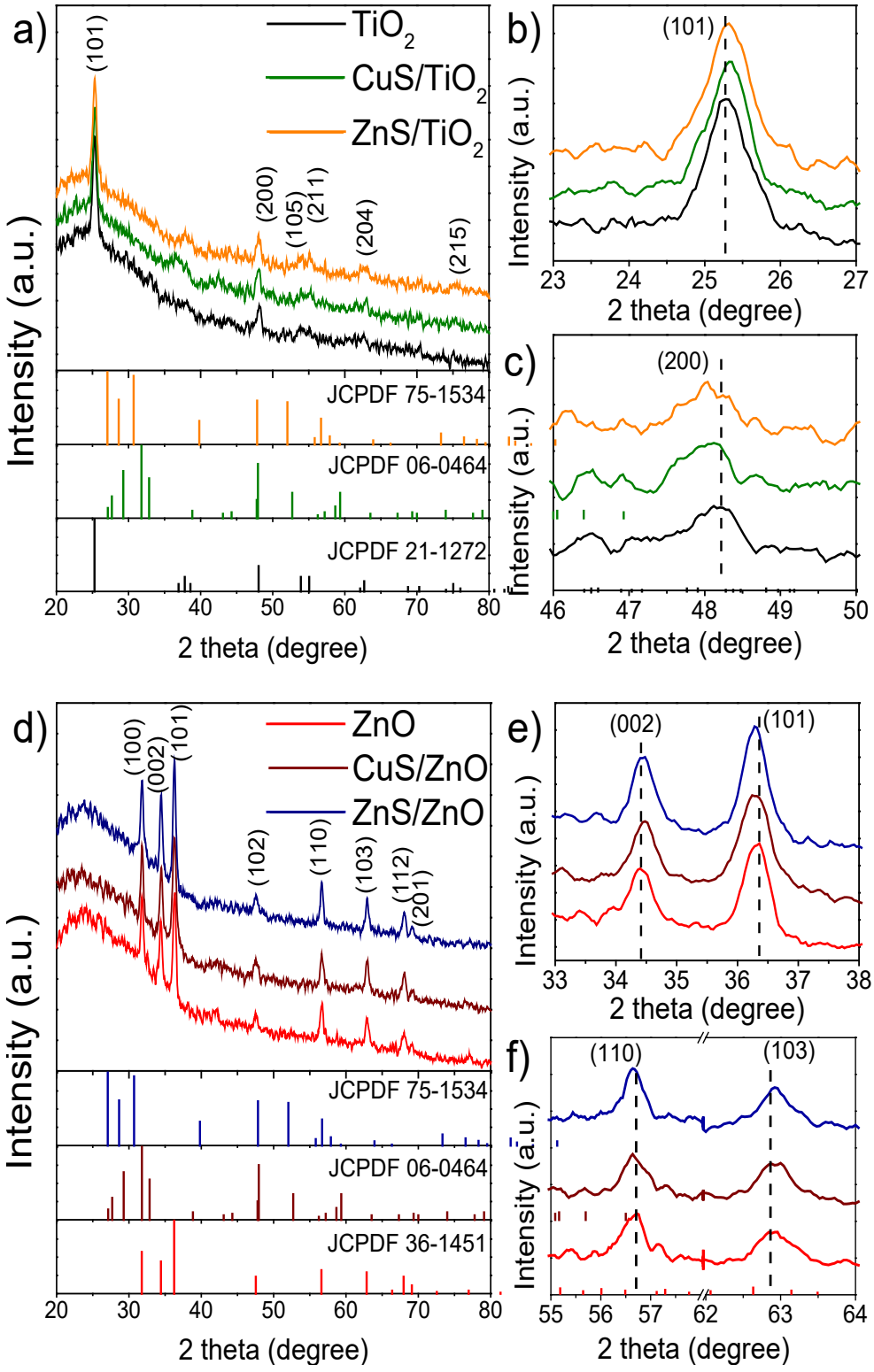

Fig. 1. a) - c) XRD patterns of TiO_2, ZnS/TiO_2, and CuS/TiO_2, d) – f) ZnO, ZnS/ZnO y CuS/ZnO.

3.2. Raman spectroscopy

Figure 2-a) shows vibrational bands located at 144 cm^{-1} and 638 cm^{-1} of the $E_g(1)$ and $E_g(3)$ modes of the anatase phase of TiO_2. The 399 cm^{-1} peak is assigned to the $B_{1g}(1)$ mode and is the symmetric bending vibration of the O-Ti-O bonds; and the 515 cm^{-1} peak assigned to the $A_{1g}+B_{1g}$ mode; the A_{1g} mode antisymmetric bending vibration of O-Ti-O bonds [23]. In CuS/TiO_2 and ZnS/TiO_2 samples, signal displacements are observed due to a change in symmetry associated with the chemical interaction between ZnS, CuS and TiO_2, respectively [24].

Figure 2-b) shows the characteristic vibrational modes of the hexagonal wurtzite structure of ZnO [13]. The E_2 (low) vibrational mode located at ~100 cm^{-1} is associated with the Zn^{2+} sublattice [25]. The E_2 (high) - E_2 (low) mode at 330 cm^{-1} is associated with the optical transversal mode of the lattice phonons. The E_2 (high) mode signal is related to high crystallinity in the samples and is located at ~440 cm^{-1}. The band at 573 cm^{-1} is associated with the E_1(LO) of the optical longitudinal mode of the phonons [26], [27]. The shifting of the characteristic peaks of semiconductor oxides incorporating sulfides is related to substituting Cu and S ions in the crystalline structure [28], corroborating the X-ray observations.

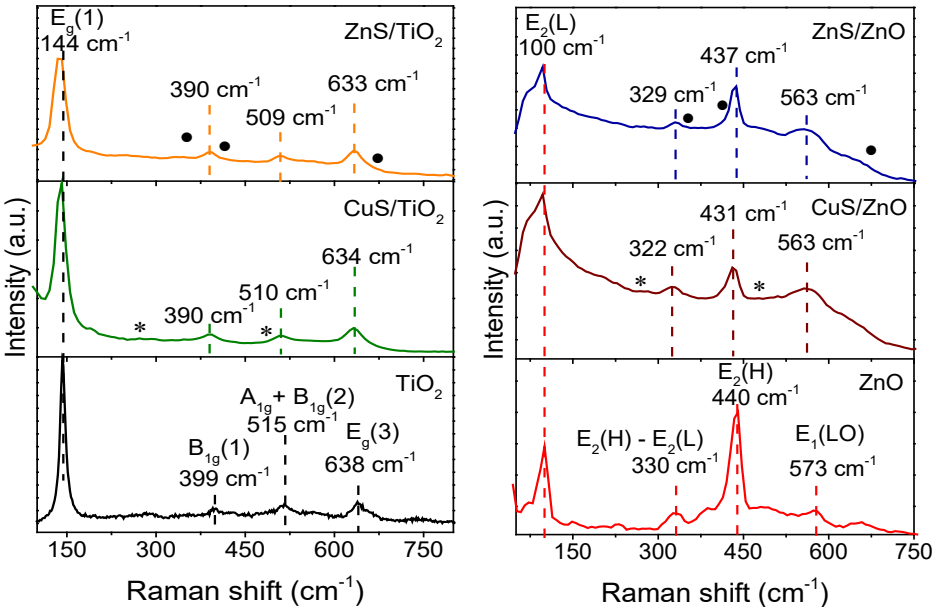

Fig. 2. Raman spectra for a) TiO_2 and b) ZnO, and their respective composites, ZnS and CuS.

Figure 3 shows the FWHM behavior of the Raman spectrum in the preferential direction of TiO_2 (144 cm^{-1}) and ZnO (440 cm^{-1}). Since the values decrease, the heterojunctions have better crystallinity than the oxide films [12].

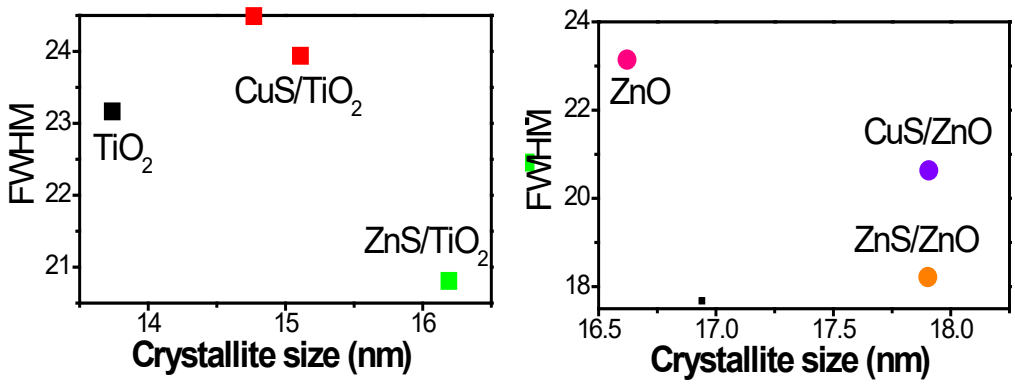

Fig. 3. FWHM variation vs. crystal size for films composites, corresponding to the Raman band at 144 cm^{-1} y 440 cm^{-1}, attributable to TiO_2 and ZnO, respectively and their composites.

3.3. UV-Vis spectroscopy

In the UV-Vis spectra shown in Figure 4, it is observed that CuS/TiO_2 extends the absorption range to the visible light region since CuS nanoparticles contribute to the displacement due to band doubling [29]. Figure 4 shows that ZnO transmits 73-87% in the visible region, and the transmittance of CuS/ZnO decreases concerning ZnO (52-73%). In addition, a displacement in the absorption of ZnS/TiO_2 attributed to the doubling of bands in the composite material is observed [24]. The ZnS/ZnO spectra show a slight displacement in the absorption caused by energetic states generated with the coupling (83% in visible).

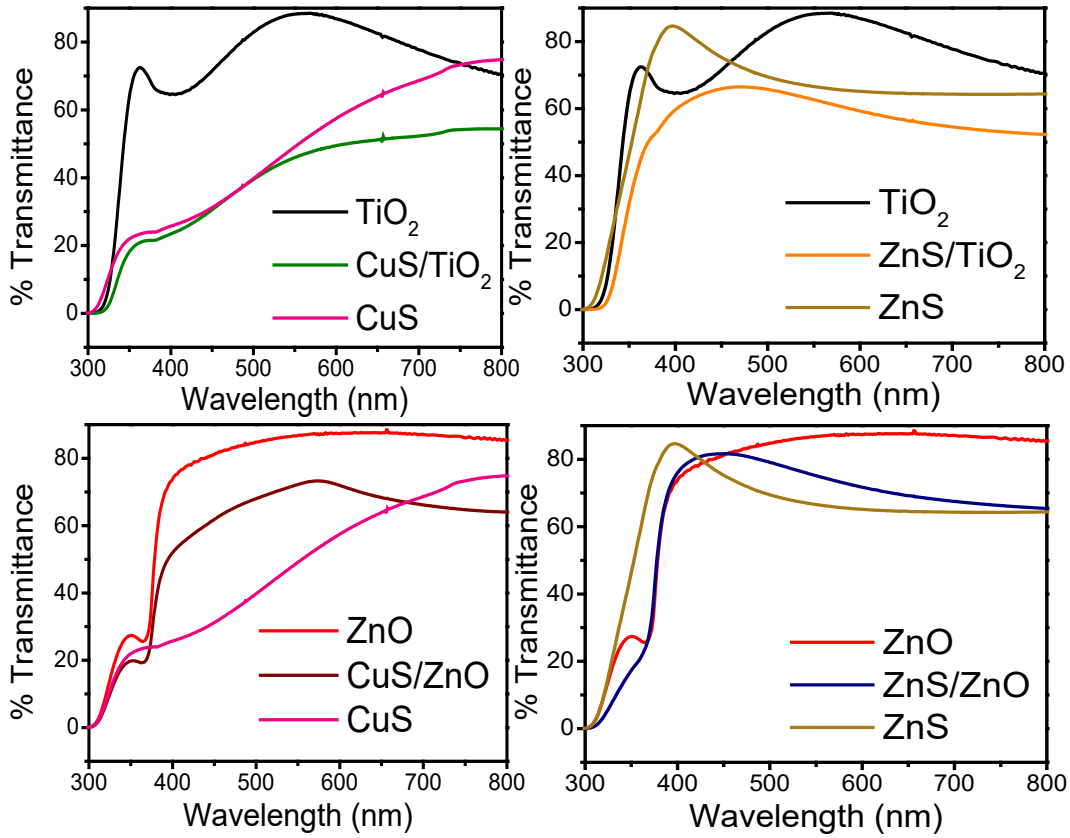

Fig. 4. Films transmittance spectra based on TiO_2 y ZnO.

The bandgap of the films was calculated using the Tauc model (Eq. 2), extrapolating the straight $(\alpha hv)^n$ vs hv [30].

$$\propto = \frac{k(hv-E_g)^n}{hv} \tag{2}$$

where k is Planck's constant, hv is the photon energy (eV), $n = 1/2$ y $n = 2$, for ZnO and TiO_2, respectively. The decrease in the bandgap of the couplings for the pure compounds is attributed to the incorporation of energetic states [31]. Table 2 summarizes the refractive index values and the porosity calculated using the Wolfe method. The results for the compounds with CuS show that the refractive index decreases when the porosity of the films increases (See Figure 5) [30], [32].

Table 2. Optical and Surface properties of oxides and compositos samples.

Sample	Bandgap (eV)	Refractive index (n)	Porosity (%)	Roughness (%)
TiO_2	3.4	1.5141	75.38	1.507
CuS/TiO_2	3.36	1.5909	70.83	30.667
ZnS/TiO_2	3.35	1.5129	75.45	2.262
ZnO	3.2	1.5170	68.09	3.533
CuS/ZnO	2.94	1.6164	66.01	19.15
ZnS/ZnO	3.07	1.5830	68.00	3.274

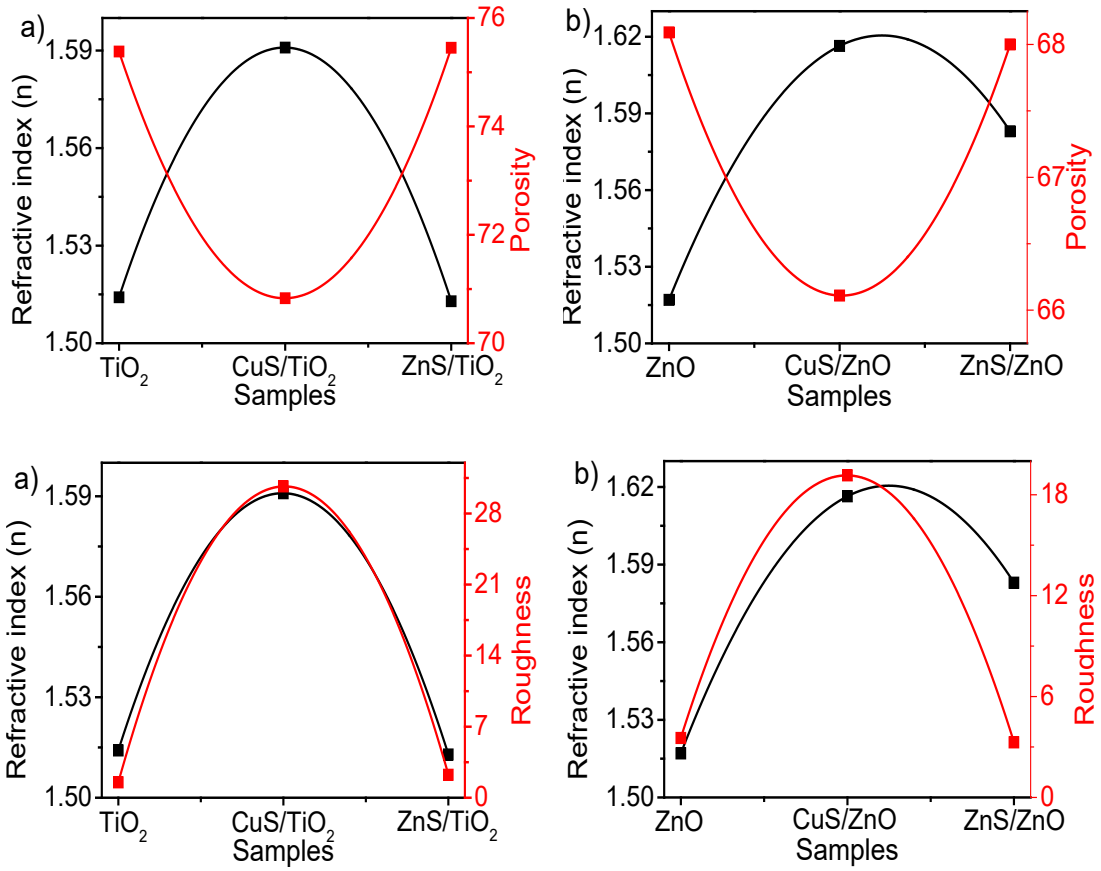

Fig. 5. Variation of refractive index and porosity films based on TiO_2 y ZnO.

3.4. Atomic force microscopy (AFM)

The roughness of the samples is observed in the AFM micrographs (Figure 6). The roughness values are 1,507 nm, 2,262 nm, and 30 nm for TiO2, ZnS/TiO_2, and CuS/TiO_2, respectively. The difference in the roughness values is attributed to the nucleation of the particles and is related to the results obtained for the refractive index (Figure 5) [33], [34], [35], [36]. For the samples with ZnO, the roughness obtained is similar to that shown by the films with TiO2: CuS/ZnO > ZnO > ZnS/ZnO.

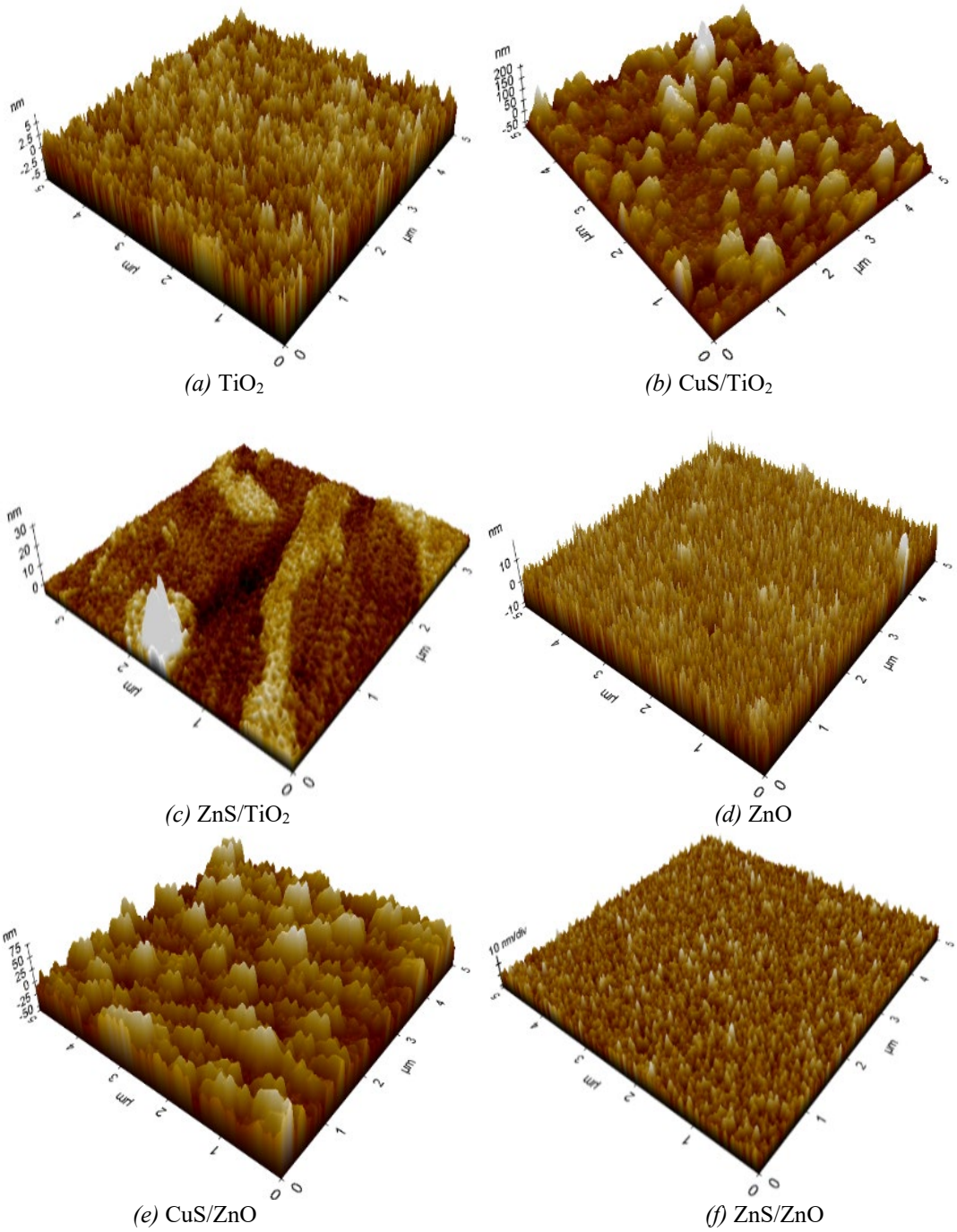

Fig. 6. 3D of AFM imaging for films based on TiO_2 and ZnO.

3.5. Photoelectrochemical evaluation

Figure 7 shows the photoelectric response of films under visible light irradiation. The results show a weak TiO_2 signal attributed to the band gap. The CuS/TiO_2 film has higher electrical conduction than TiO_2 due to the combination of bands that induce photo-induced charge separation [37]. However, the CuS/ZnO sample exhibits the most increased electrical conduction due to decreased film porosity. In addition, this film presents a decrease in resistivity due to the incorporation of CuS, improving the current collection in the electrodes. Therefore, CuS nanoparticles enhance the separation of photo-induced electron-hole pairs [38].

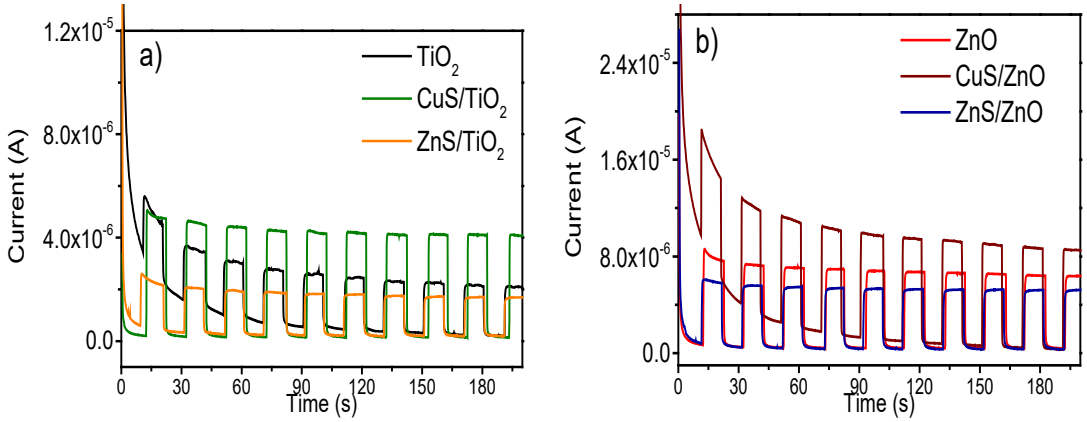

Fig. 7. Photoresponse for a) TiO_2—, CuS/TiO_2— ZnS/TiO_2—; b) ZnO—, CuS/ZnO—, ZnS/ZnO—

4. Conclusions

Experimental results obtained showed that the fabrication of thin films with CuS and ZnS supports by metal oxides (TiO_2 y ZnO) are benefited by the whole samples, indicating a decrease of energy gaps due the size change of crystals. As wel as, increase a considerable way of absorb the visible spectrum because of the new creations of energetics levels that helps enhancing factors like electrical and optical. This as a result of an excellent homogeneity of the material roughness, besides all that has CuS present a major roughness, generating a better refraction and a photoelectric response due to the accumulation of photo-injected electrons in the conduction band. The response to light to conduct electricity of the composites coupled with CuS is greater than those coupled with ZnO.

Meanwhile, these results establish that the dense, smooth and homogeneity obtained by Dip-Coating and evaporation were such effective in order to decrease considerably the resistance to charge transfer.

Acknowledgments

This research is financial supported by Council of Science and Technology of the State of Tabasco through the funds PRODECTI-2022-01/56.

References

[1] S. F. Shaikh, H.-C. Kwon, W. Yang, R. S. Mane, and J. Moon, J Alloys Compd, vol. 738, 405–414 (2018); https://doi.org/10.1016/j.jallcom.2017.12.199
[2] D. Dahlan, S. K. M. Saad, A. U. Berli, A. Bajili, and A. A. Umar, Physica E Low Dimens Syst Nanostruct, vol. 91, 185–189 (2017); https://doi.org/10.1016/j.physe.2017.05.003
[3] I. Iwantono, S. K. M. Saad, R. Yuda, M. Y. Abd Rahman, and A. A. Umar, Superlattices Microstruct, vol. 123, 119–128 (2018); https://doi.org/10.1016/j.spmi.2018.05.041
[4] Q. Chen, S. Wu, and Y. Xin, Chemical Engineering Journal, vol. 302, 377–387 (2016); https://doi.org/10.1016/j.cej.2016.05.076
[5] C. Zhou, Q. Chen, G. Wang, A. Guan, L. Zhou, N. Huang, J. Xu, Journal of Electroanalytical Chemistry, vol. 780, 271–275, (2016); https://doi.org/10.1016/j.jelechem.2016.09.039
[6] L. Wang, X. Gu, Y. Zhao, Y. Qiang, C. Huang, and J. Song, Vacuum, vol. 148, 201–205 (2018); https://doi.org/10.1016/j.vacuum.2017.11.023

[7] B. Ünlü, S. Çakar, and M. Özacar, Solar Energy, vol. 166, 441–449 (2018); https://doi.org/10.1016/j.solener.2018.03.064
[8] M. P. A. Muthalif, C. D. Sunesh, and Y. Choe, J Photochem Photobiol A Chem, vol. 358, 177–185 (2018); https://doi.org/10.1016/j.jphotochem.2018.03.013
[9] U. Shamraiz, R. A. Hussain, and A. Badshah, J Solid State Chem, vol. 238, 25–40 (2016); https://doi.org/10.1016/j.jssc.2016.02.046
[10] X.-S. Hu, Y. Shen, L.-H. Xu, L.-M. Wang, L. Lu, and Y. Zhang, Appl Surf Sci, vol. 385, 162–170 (2016); https://doi.org/10.1016/j.apsusc.2016.05.089
[11] F. Ongul, U. Ulutas, S. A. Yuksel, S. S. Yesilkaya, and S. Gunes, Synth Met, vol. 220, 1–7 (2016); https://doi.org/10.1016/j.synthmet.2016.05.017
[12] N. R. Mathews, E. R. Morales, M. A. Cortés-Jacome, and J. A. T. Antonio, Solar energy, vol. 83, no. 9, pp. 1499–1508 (2009); https://doi.org/10.1016/j.solener.2009.04.008
[13] A. A.-G. Farrag and M. R. Balboul, J Solgel Sci Technol, vol. 82, pp. 269–279 (2017); https://doi.org/10.1007/s10971-016-4277-8
[14] R. Vasanthapriya, N. Neelakandeswari, K. Uthayarani, and M. Chitra, "Effect of pH on the morphology of TiO2 nanostructures," *Dig J Nanomater Biostruct*, vol. 18, no. 2, pp. 767–771, Apr. 2023, https://doi.org/10.15251/DJNB.2023.182.767
[15] H. Ennaceri, M. Boujnah, A. Taleb, A. Khaldoun, R. Sáez-Araoz, A. Ennaoui, A. E. Kenz, A. Benyoussef, Int J Hydrogen Energy, vol. 42, no. 30, pp. 19467–19480 (2017); https://doi.org/10.1016/j.ijhydene.2017.06.015
[16] G. A. Velázquez-Nevárez, J. R. Vargas-Garcia, J. Aguilar-Hernandez, O. E. Vega-Becerra, F. Chen, Q. Shen, L. Zhang, Materials Research, vol. 19, pp. 113–117 (2016); https://doi.org/10.1590/1980-5373-MR-2016-0808
[17] J. Tyagi, H. Gupta, and L. P. Purohit, J Alloys Compd, vol. 880, 160480, (2021); https://doi.org/10.1016/j.jallcom.2021.160480
[18] F. Zhou, Z. Zhang, Y. Jiang, G. Yu, Q. Wang, and W. Liu, Journal of Physics and Chemistry of Solids, vol. 144, p. 109512, (2020); https://doi.org/10.1016/j.jpcs.2020.109512
[19] M. Duta, L. Predoana, J.M. Calderon-Moreno, S. Pedra, M. Anastasescu, A. Marin, I. Dascalu, P. Chesler, C. Hornoiu, M. Zaharescu, P. Osiceanu, M. Gartner, Mater Sci Semicond Process, vol. 42, 397–404, (2016); https://doi.org/10.1016/j.mssp.2015.11.004
[20] V. S. Vinila1, R. Jacob, A. Mony, H. G. Nair, S. Issac, S. Rajan, A. S. Nair, D. J. Satheesh, J. Isac, Crystal Structure Theory and Applications, vol. 3, no. 03, p. 57, (2014); https://doi.org/10.4236/csta.2014.33007
[21] T. T. Loan, V. H. Huong, V. T. Tham, and N. N. Long, Physica B Condens Matter, vol. 532, pp. 210–215, (2018); https://doi.org/10.1016/j.physb.2017.05.027
[22] L. Qiao, F. Xie, M. Xie, C. Gong, W. Wang, and J. Gao, Transactions of Nonferrous Metals Society of China, vol. 26, no. 8, pp. 2109–2116, (2016); https://doi.org/10.1016/S1003-6326(16)64325-X
[23] T. T. Loan, N. A. Bang, V. H. Huong, and N. N. Long, Opt Mater (Amst), vol. 69, pp. 30–37, (2017); https://doi.org/10.1016/j.optmat.2017.04.005
[24] Y. Xiaodan, W. Qingyin, J. Shicheng, and G. Yihang, Mater Charact, vol. 57, no. 4–5, pp. 333–341, (2006); https://doi.org/10.1016/j.matchar.2006.02.011
[25] G. G. Miranda, R. L. de Sousa e Silva, H. V. dos Santos Pessoni, and A. Franco, Physica B Condens Matter, vol. 606, p. 412726, (2021); https://doi.org/10.1016/j.physb.2020.412726
[26] P. Sathish, N. Dineshbadu, K. Ravichandran, T. Arun, P. Karuppasamy, M. SenthilPandian, P. Ramasamy, Ceram Int, vol. 47, no. 19, pp. 27934–27941, (2021); https://doi.org/10.1016/j.ceramint.2021.06.224
[27] T. T. H. Pham, X. H. Vu, T. T. Trang, N. X. Ca, N. D. Dien, P. V. Hai, N. T. H. Lien, N. T. Nghia, T. T. K. Chi, Opt Mater (Amst), vol. 120, p. 111460, (2021); https://doi.org/10.1016/j.optmat.2021.111460
[28] K. Kasirajan, L. Bruno Chandrasekar, S. Maheswari, M. Karunakaran, and P. Shunmuga Sundaram, Opt Mater (Amst), vol. 121, p. 111554, (2021); https://doi.org/10.1016/j.optmat.2021.111554
[29] L. Gao, J. Du, and T. Ma, Ceram Int, vol. 43, no. 12, pp. 9559–9563, (2017); https://doi.org/10.1016/j.ceramint.2017.04.093

[30] N. M. Ravindra, P. Ganapathy, and J. Choi, Infrared Phys Technol, vol. 50, no. 1, pp. 21–29, (2007); https://doi.org/10.1016/j.infrared.2006.04.001
[31] D. Li and C. Pan, *Progress in Natural Science: Materials International*, vol. 22, no. 1, pp. 59–63, (2012); https://doi.org/10.1016/j.pnsc.2011.12.010
[32] F. Mesa, V. Ballesteros, and A. Dussan, Univ Sci (Bogota), vol. 19, no. 2, pp. 123–131, (2014); https://doi.org/10.11144/Javeriana.SC19-2.ccop
[33] M. I. Khan, S. Imran, M. Saleem, and S. U. Rehman, Results Phys, vol. 8, pp. 249–252, (2018); https://doi.org/10.1016/j.rinp.2017.12.030
[34] A. El Hamidi, K. Meziane, A. El Hichou, T. Jannane, A. Liba, J. El Haskouri, P. Amorós, A. Almaggoussi, Optik (Stuttg), vol. 158, pp. 1139–1146, (2018); https://doi.org/10.1016/j.ijleo.2018.01.011
[35] Y. Zhang, B. Huang, P. Li, X. Wang, and Y. Zhang, Tribol Int, vol. 58, pp. 7–11, (2013); https://doi.org/10.1016/j.triboint.2012.09.004
[36] A. Sreedhar, H. Jung, J. H. Kwon, J. Yi, Y. Sohn, and J. S. Gwag, Journal of Electroanalytical Chemistry, vol. 804, pp. 92–98, (2017); https://doi.org/10.1016/j.jelechem.2017.09.045
[37] Z. Li, Y. Qu, G. He, M. Humayun, S. Chen, and L. Jing, *Appl Surf Sci*, vol. 351, pp. 681–685, (2015); https://doi.org/10.1016/j.apsusc.2015.05.190
[38] J. Lv, Q. Zhu, Z. Zeng, M. Zhang, J. Yang, M. Zhao, E. Wang, Y. Cheng, G. He, Z. Sun, Journal of Physics and Chemistry of Solids, vol. 111, pp. 104–109, (2017); https://doi.org/10.1016/j.jpcs.2017.07.017